PROBLEMY MECHATRONIKI
UZBROJENIE, LOTNICTWO, INŻYNIERIA BEZPIECZEŃSTWA

ISSN 2081-5891

8, 1 (27), 2017, 39-54

PROBLEMS OF MECHATRONICS
ARMAMENT, AVIATION, SAFETY ENGINEERING

Examination of the Explosion Strike Factors of a Thermobaric Warhead

Andrzej DŁUGOŁĘCKI, Andrzej FARYŃSKI*, Tomasz KLEMBA, Łukasz SŁONKIEWICZ, Zbigniew ZIÓŁKOWSKI

Air Force Institute of Technology
6 Księcia Bolesława Street, 01-494 Warsaw, Poland
**Corresponding author's e-mail address: andrzej.farynski@itwl.pl*

Received by the editorial staff on 1 July 2015.
The reviewed and verified version was received on 23 February 2016.

DOI 10.5604/01.3001.0009.8993

Abstract: This paper presents the measurement method and results applicable to the pressure pulses and thermal effects generated by an explosion of an unguided thermobaric rocket missile warhead. The determination results include the shock wave pressure and velocity, the TNT equivalents of the thermobaric warheads, and the personnel strike radii of the shock wave. An estimation of the temperature increase rates at the shock wave front was also undertaken.
Keywords: mechanics, thermobaric explosion, shock wave, shock wave velocity, pressure pulse

1. INTRODUCTION

Thermobaric munitions have been enjoying increasing popularity in recent years. Thermobaric explosives have been a subject of many scientific papers, including in Poland.

A wide review of thermobaric ammunition design works in Poland is presented in [1], while examples from other countries are discussed in [2].

Air Force Institute of Technology (AFIT) has been testing a derivative type of FAE (fuel-air explosion) ammunition since the beginning of the 1990s. Some of this research is explained in [3]. The strike effect of RA-79 conventional warheads [4] for unguided air-to-surface missiles was tested with the methodology applied for testing of the M151 warheads [5].

This study contains a description of the testing for an unguided rocked missile thermobaric warhead. The tests were intended to provide the parameter data of the explosion shock wave and its strike effect, the thermal effects of the explosion within the near explosion blast radius and the spatial symmetry of the explosion effects. The tests were undertaken with a system approximate to the one applied in [4], including the temperature sensors developed at AFIT for measurement with a time resolution, an improvement over other thermocouple systems described in [5].

In the investigated thermobaric warhead design, a charge of classic high explosive material (CHE) is encased in a layer of pulverized incendiary material (IM), either an aluminium powder or magnesium powder mixed with a stabilizing matrix. The detonation of this warhead type is a two-stage process.

Stage 1 is the detonation of the CHE charge, during which the CHE reacts and its reaction products are dispersed (atomized). The CHE reaction products include, if the oxygen balance is negative, carbon monoxide, hydrogen, carbon black and coal dust. This is concomitant with the dispersal of the IM. The flammable reaction products of the CHE and the atomized IM are mixed with air.

During this mixing (Stage 2), the metallic particulates, which are heated to a high temperature, are subject to violent combustion in the air and initiate afterburning of the CHE reaction products, resulting in the blast wave. The overpressure (relative to the barometric pressure) generated by the blast wave is recorded as a pulse with a positive phase and a negative phase (vacuum). The metallic particulate combustion process generates an additional, highly intense heat flux which affects the environment (resulting in fire and body burns) and, unlike a charge of pure CHE, increases the positive phase pulse duration. The replacement of the oxygen in the air with the metal oxides produced by the afterburning intensifies the negative (vacuum) phase.

As shown later, the recorded overpressure pulses generated by the blast waves featured fronts, the increase in time of which was shorter than the sampling period of the recording oscilloscope; therefore, the blast waves were still described as “shock waves”.

2. DIAGRAM OF THE SHOCK WAVE FRONT OVERPRESSURE & TEMPERATURE MEASUREMENT SYSTEM

Figure 1 shows the arrangement of the tested thermobaric warhead as well as the measurement and recording devices in a horizontal planar projection.

The tested thermobaric warhead was positioned at height H = 1.6 m above the terrain level and with its axis of symmetry perpendicular to the terrain surface. The tested thermobaric warhead carried approx. 0.2 kg of CHE with an approximate explosion heat value of 5 MJ/kg, and approx. 2 kg of the additional IM (aluminium dust + isopropyl alcohol), encasing the CHE charge in a cylindrical symmetry. The CHE charge was initiated from the thermobaric warhead front.

The overpressure at the generated shock wave (SW) front was measured with two piezoelectric sensors, PS1 and PS2, which are designated here (including in the graphs) as Sensor 1 and Sensor 2, respectively. The two sensors were located at H = 1.6 m over the terrain level and at the following distances from the thermobaric warhead:

- r_{p1} = 5 m for Sensor 1 (to enable recording of specific volumetric explosion phases);
- r_{p2} = 20 m for Sensor 2 (to allow approaching the warhead charge explosion as a point charge explosion).

The applied piezoelectric pressure sensors were PCB Piezotronics in pencil-type cases (i.e. Pencil Probe 137A22 and 137A23). The pencil-type cases were cylindrical nacelles with their tapered tips aimed towards the tested thermobaric warhead. The active surfaces of the sensors in the cases were located on the nacelle side wall, in parallel to the shock wave direction of propagation. This configuration makes the impact of explosion-propelled particulates against the pencil-type cases very unlikely. If such an impact occurs, it can be verified.

The thermal effect of the thermobaric warhead explosion was recorded with resistive temperature sensors developed by AFIT [6].

The sensors were located at H = 1.6 m over the terrain level and at the following distances from the thermobaric warhead:

- 5 m for sensor TS1 (intended to enable recording of air temperature changes near the afterburning reaction zone);
- 20 m for sensor TS2 (intended to enable recording of air temperature changes outside the shock wave front).

The sensor output signals were recorded with digital oscilloscopes labelled Os1 and Os2 and triggered with pulse generator P; the pulse generator was triggered by a short-circuit-type starting sensor SS, located approximately 1 mm from the outer surface of the thermobaric warhead.

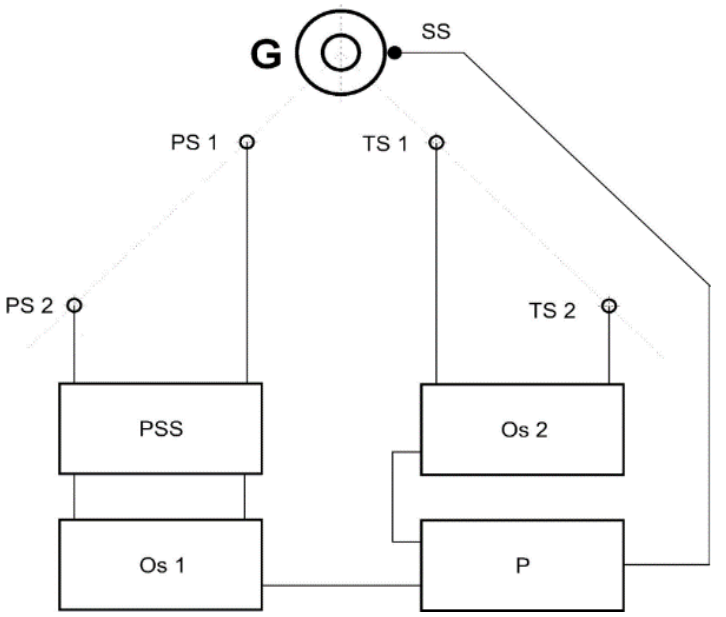

Fig. 1. Diagram of the measurement system:
G – thermobaric warhead; SS – starting sensor; PS1 – first pressure sensor;
PS2 – second pressure sensor; TS1 – first temperature sensor, TS2 – second temperature sensor; PSS – pressure sensor power supply; Os1, Os2 – digital oscilloscopes;
P – starting pulse generator

3. VISUALISATION OF THE DISPERSAL OF THERMOBARIC WARHEAD EXPLOSION PRODUCTS

The process of detonation product dispersal was recorded with a Phantom V-711 slow-motion camera, operating at 25,000 fps. The video was recorded with the thermobaric warhead installed on a wooden cradle with the axis of symmetry in the horizontal plane. The LOS camera was aimed nearly in parallel to the warhead's axis of symmetry.

Figure 2 shows examples of the still frames from the video with the warhead explosion phases. Based on the video recording, the following conclusions can be made:

- Up to approx. +1 ms from the process start (t_0) – during Phase 1 – the glowing region expanded with its high cylindrical symmetry retained (Fig. 2a) (the dispersal symmetry of thermobaric explosion products is a major contributor to the stable and repeatable strike effect of the warhead). The glow consisted of the CHE explosion products and the non-converted IM being dispersed; after approx. 0.5 ms, the circular envelope of the glowing area began to develop separate fluxes (Fig. 2b).

- At approx. +1 ms from t_0, the dark circumaxial area (Fig. 2c) began to expand; this was most likely the vacuum area within the cloud, the symmetry of which was between cylindrical and spherical; air was induced into this dark area from the outside and along the system axis, providing turbulence for the IM dispersal and mixing with the IM.
- At approx. +2 ms from t_0, the dark circumaxial area was completely covered by a mixture with a less intense glow; the process of mixing (mainly metallic particulates with air) and glow abatement grew to cover the entire area originally occupied by the intense glow (Fig. 2d); this process lasted up to approx. +7 ms from t_0.

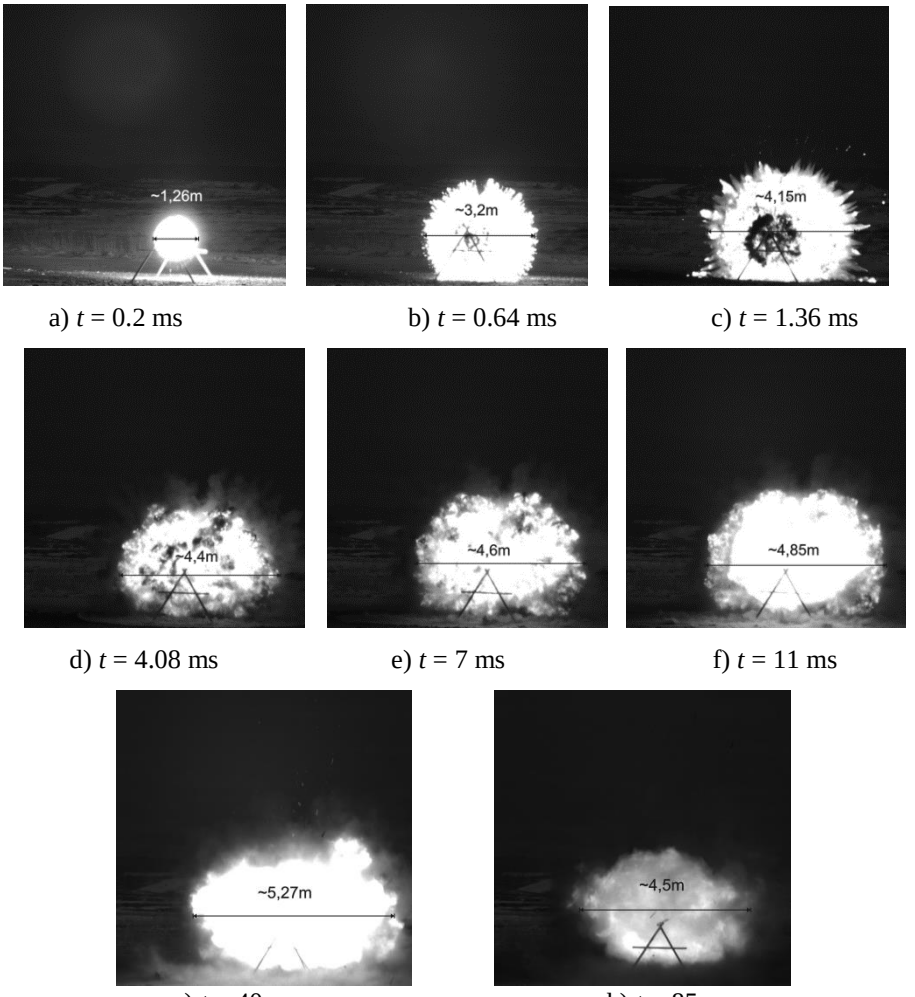

a) t = 0.2 ms b) t = 0.64 ms c) t = 1.36 ms

d) t = 4.08 ms e) t = 7 ms f) t = 11 ms

g) t = 40 ms h) t = 85 ms

Fig. 2. Selected video still frames of the thermobaric warhead explosion

- At approx. +7 to +8 ms form t_0, the IM-air mixture was ignited (Fig. 2e) – Phase 2. This was an intense reaction with a second onset of intense glowing and expansion; this was a relatively long-lasting phase (Figs. 2e, f, g) and ended approx. +0.1 s (Fig. 2h), and between +20 ms and +40 ms from explosion initiation, the image of the glowing area changed insignificantly.

Note the pulsing effect of the glowing area diameter caused by the vacuum pressure areas within the explosion zone.

The maximum diameter of the glowing area, estimated by the video still frames, was approx. 5.5 m at +40 ms from explosion initiation, and the glowing area expansion velocity (mass velocity) at the same time was approx. 15 m/s.

4. MEASUREMENT OF SHOCK WAVE OVERPRESSURE AND PROPAGATION VELOCITY

The applied method of measurement synchronisation enabled recording of overpressure Δp, with times t_{p1} and t_{p2} after SW contact with specific sensors.

Figure 3 shows an example of the overpressure trends recorded by both pressure sensors as a function of time. Time $t = 0$ is the time of triggering by sensor SS (explosion initiation).

The respective SW propagation parameters are listed in Tables 1 and 2. Δp_{imax} is the maximum recorded overpressure at r_{pi}, i = 1, 2. The mean SW velocity values at the sections from the warhead to PS1 and from PS1 to PS2 were, respectively: $v_{p1} = r_{p1}/ t_{p1}$ and $v_{p2} = (r_{p2} – r_{p1}) / (t_{p2} – t_{p1})$. The values v_{p1} are approximate to the SW velocity values (approx. 800 m/s) at $r_{p1} = 5$ m shown on a trend plot in Fig. 4 and obtained by tracking the SW front progression against the horizon recorded by the slow-motion video camera. The oblique orientation of the SW front against the horizon resulted in overestimation of the determined trend values. $\tau_{1,2+}$ are the duration times of the pressure pulse positive phase.

The pressure and wave velocity measurements can be verified with an approximate relationship for a weak flat SW in air:

$$\Delta p_{1,2max} \approx \rho_P \, v_{p1,2} \, (v_{p1,2} - c_S)$$

with: $\rho_P = 1.225$ kg/m^3 – air density,

$c_S = 340$ m/s – sound velocity in air under normal conditions.

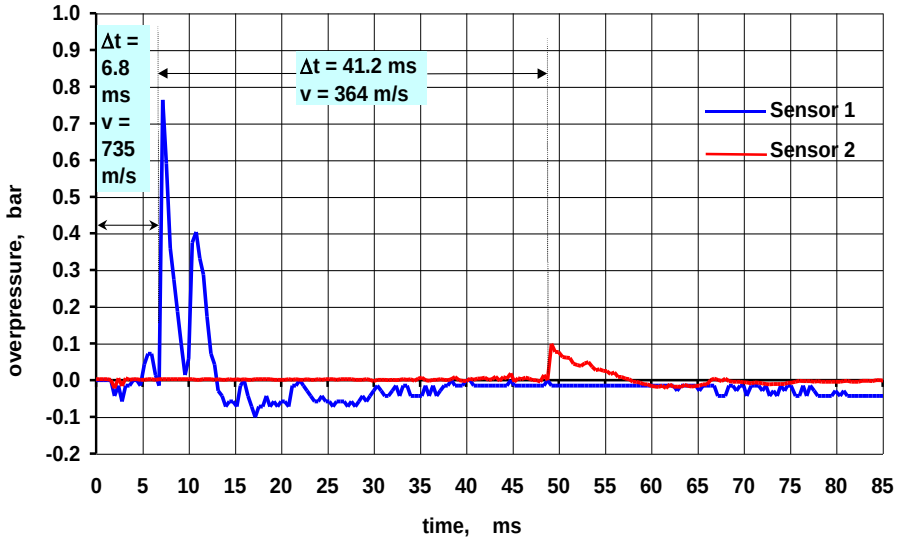

Fig. 3. Overpressure trends of the SW front at 5 m (Sensor 1) and 20 m (Sensor 2) from the thermobaric warhead, Explosion 1; mean SW velocity values at specific sections were calculated

This relationship can only be applied to the sensor located further away from the thermobaric warhead (r_{p2} = 20 m), because the situation for the closer sensor (r_{p1} = 5 m) features overpressure pulses very different from the typical pulses from a single shock wave, which is due to the complex multi-phase nature of the explosion. Table 2 lists the evaluated overpressure values as Δp_{2eval}.

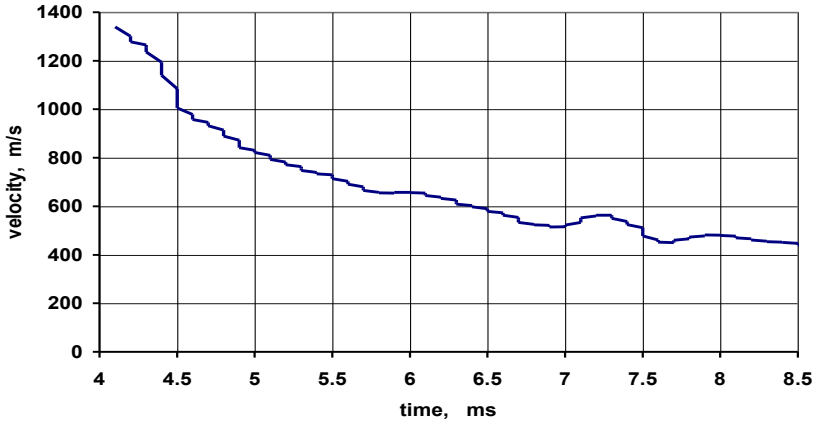

Fig. 4. SW front velocity vs. propagation time, as determined using still frames from the slow-motion camera

Table 1. Overpressure pulse parameters related to the SWs recorded with sensor PS1

	r_{p1} [m]	t_{p1} [ms]	v_{p1} [m/s]	Δp_{1max} [bar]	τ_{1+} [ms]
Explosion 1	5	6.8	735	0.765	6.0
Explosion 2	5	6.2	806	0.693	6.2
Explosion 3	5	6.2	806	1.096	6.4
Explosion 4	5	6.2	806	0.721	6.0

Table 2. Pressure pulse parameters related to the SWs recorded with sensor PS2, complete with determined TNT equivalent values

	r_{p2} [m]	t_{p2} [ms]	v_{p2} [m/s]	Δp_{2max} [bar]	Δp_{2eval} [bar]	τ_{2+} [ms]	Q_τ [kg]	Q_p [kg]
Explosion 1	20	48.0	364	0.099	0.107	8.2	3.3	2.7
Explosion 2	20	48.0	359	0.101	0.086	8.1	3.1	3.0
Explosion 3	20	48.0	359	0.096	0.086	8.2	3.3	2.5
Explosion 4	20	48.0	359	0.092	0.086	8.2	3.3	2.5

The total duration of a complex-form overpressure pulse at 5 m from the explosion epicentre was approx. 6 ms, whereas the overpressure pulse generated by a CHE charge with the same TNT equivalent should last approx. 4 ms (see Section 5). The overpressure pulses recorded by Sensor 2, located 20 m from the detonated warhead, featured typical trends at an amplitude of approx. 100 hPa (0.1 bar) and a positive pressure phase duration of approx. 8 ms.

5. TNT EXPLOSION EQUIVALENT

The relevant formulas [7] link TNT explosive charge equivalent Q with the maximum overpressure value at the SW front (Sadowski's formula):

$$\Delta p_{1,2max} = A\,(Q^{1/3} / r_{p1,2}) + B\,(Q^{1/3} / r_{p1,2})^2 + C\,(Q^{1/3} / r_{p1,2})^3 \quad (1)$$

with: $$A = 1.06,\ B = 4.3,\ C = 14.0 \quad (2)$$

and the pressure pulse positive phase duration:

$$\tau_{1,2+} = 0.0015\,(r_{p1,2})^{1/2}\,Q^{1/6} \quad (3)$$

In the formulas, $\Delta p_{1,2max}$ is expressed in bars (1 bar = 100 kPa), Q is expressed in kilograms, $r_{p1,2}$ is expressed in metres, and $\tau_{1,2+}$ is expressed in seconds. These factors are true for a surface (contact) explosion and an above-ground (airborne) explosion, where the distance to a measurement sensor exceeds the suspension elevation of the explosive charge, $r_{p1,2} > H$ [7].

This condition was met for r_{p1} and r_{p2}; however, given that r_{p1} = 5 m, the recorded trends Δp_1 did not feature the "classic" form of a positive pressure monopulse, followed by a vacuum monopulse. The TNT equivalent values were determined only with the overpressure trends recorded with r_{p2} = 20 m, i.e. sensor PS2, located further away from the explosion epicentre. Given such a small distance, the Mach wave effect can be practically omitted.

From the sensor values in Table 2, the TNT equivalent Q values were derived (Q_p – from Δp_{2max}, and Q_τ – from τ_{2+}), which are also listed in Table 2. The mean values of the TNT equivalents were $Q \approx 3.0 \pm 0.5$ kg TNT.

The formula (1) also revealed that the 0.2 kg CHE charge of the tested barometric warhead to disperse the IM and initiate the IM air mixture could produce an overpressure of 0.23 bar 5 m from the explosion epicentre without energy loss for propelling the IM. Given this, the first pressure peak reading corresponding to the distance in Fig. 3 should be considered as generated by the explosive incineration of the IM powder dispersed in the air, with the combustion product being aluminium oxide (Al_2O_3) in the form of a white dust. The subsequent peak readings were affected by oscillations in the explosion cloud.

The factors (2) were obtained by averaging a large quantity of experimental data. This method imposes an additional error on the determination of Q with (1). This error was estimated in [3], which involved testing the explosion of an aerosol-dispersed liquid (ethylene oxide, EOT) with an initial mass of 50 kg and 2 × 50 kg. For comparison, the tests featured a single explosion of a 50 kg TNT charge in a lightweight casing with a size <0.5 m, and the same geometry as the tested EOT charge (H = 2.3 m, distance to pressure sensors r_p = 15, 30 and 44 m). The maximum overpressure values recorded in 3 points allowed this determination with (1):

$$A = 1.362,\ B = -2.599,\ C = 37.74; \tag{4}$$

The radial distribution Δp_{max} with the factors in the area of interest deviated from the radial distribution calculated with (1), (2). The then-calculated TNT equivalent $Q_{(2)}$ values (with the overpressure for r_p = 44 m) from (1) with (2) were 85 kg for the 50 kg EOT charge and 185 kg for the mean of three 2 x 50 kg EOT explosions. The respective $Q_{(3)}$ values (with the factors (4)) were 106 kg (50 kg EOT) and 227 kg (the mean of 3 explosions of the 2 x 50 kg EOT). Hence the absolute errors $[Q_{(3)} - Q_{(2)}] / Q_{(2)}$ from the factor deviations were 25 and 23%, respectively.

6. PERSONNEL STRIKE RADIUS

The SW safe radius can be expressed with the formula [3]:

$$r_B = 15\ Q^{1/3}, \qquad (r_B - [\text{m}],\ Q - [\text{kg}])$$

Zero injuries were assumed at $\Delta p \leq 0.1$ bar when the SW safe radius was determined. Given $Q = 3$ kg, the result was $r_B = 22$ m. This value roughly corresponds to the distance r_{p2}. The strike radius corresponding to $\Delta p = 0.2$ bar is approximately $r_R \approx 13$ m.

7. TEMPERATURE MEASUREMENT OUTSIDE THE BLAST WAVE FRONT

The available thermocouple version featured a minimum signal rise time of 0.1 s. This time seemed to be even longer for other thermocouple systems [5], judging by the measurement plots. Given that the phenomenon studied here lasted ~ 0.1 s, it was decided to measure temperature T in a zone close to the afterburning reaction area with proprietary resistive sensors [6] having a signal rise time that was many times shorter, i.e. of approx. 1.5 ms.

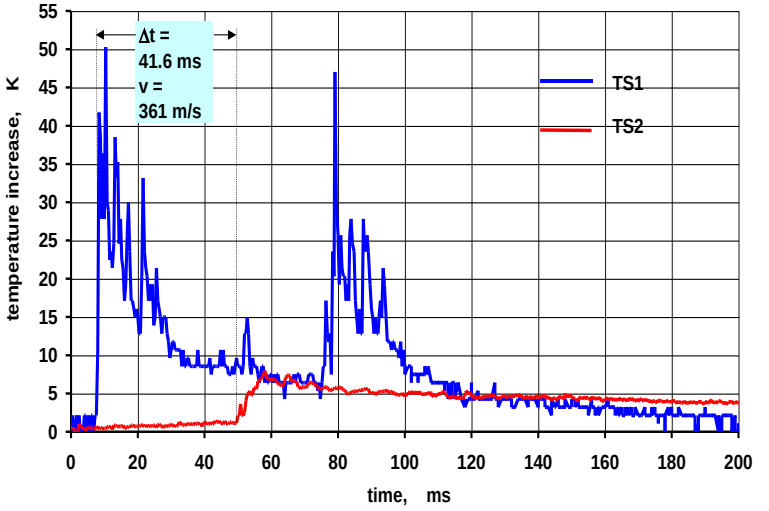

Fig. 5. Air temperature increase 5 m (Sensor TS1) and 20 m (Sensor TS2) from the detonating warhead; estimated shock wave velocity shown

The sensors were located 5 m (TS1) and 20 m (TS2) from the exploding thermobaric warhead. The element sensitive to temperature changes in the proprietary sensors was a tungsten wire, length $l_0 = 70$ mm, diameter $d_d = 45$ μm and resistance $R = R_0\ (1 + \alpha\ \Delta T)$, with $\alpha = 0.0046$ 1/K.

Given the unshielded exposure of the sensor tungsten wire to explosion product wash, the sensor distance to the explosion epicentre was limited by the ability of the mechanical strength of the tungsten wire to resist the shock blast and dispersed detonation products.

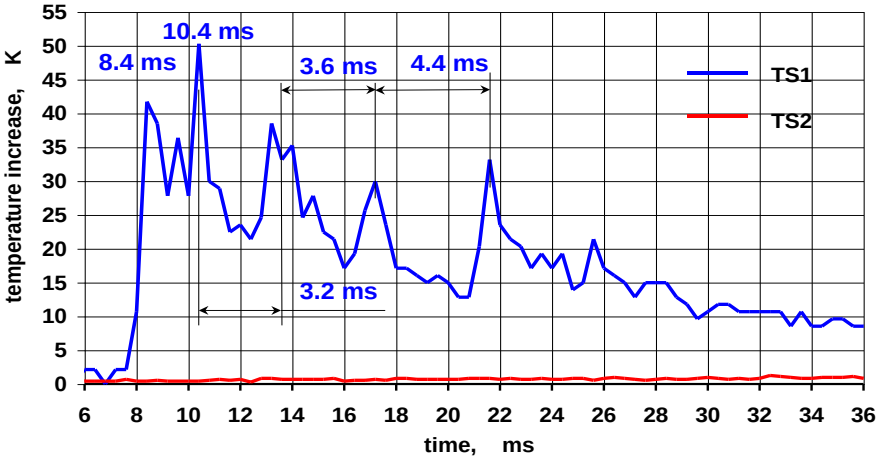

Fig. 6. Development of the initial portion of the curves in Fig. 5

The sensor output signal was proportional to

$$\Delta R / R_0 = \alpha \Delta T \tag{5}$$

The obtained temperature change records are shown in Figs. 5, 6 and 7. The records show that, unlike the overpressure effects, the duration of the thermal effects of the explosion products on the environment was extremely long.

During Explosion 1, the first recorded thermal pulse (a temperature increase by approx. 50 K) occurred at approx. +7 ms from the warhead explosion initiation time, and simultaneously with the SW front contact with Sensor TS1. The time points of the first two peaks matched the pressure peaks of the same explosion (Fig. 3). The temperature trend output by Sensor TS1 featured an oscillation period $\tau_{osc} \approx 4$ ms and a peak-valley height of 15-20 K; these oscillations abating much later than the pressure oscillations. Sensor TS1 also recorded a secondary hot air blast wave pulse at approx. +80 ms. The form of this pulse was very much like the first pulse, and with similar oscillation patterns. The secondary pulse was within the time interval of the explosion phenomenon duration, as established with the still frames from the camera. This suggests that two significantly different phases existed during Stage 2 (as called in Section 1).

During the successive explosions, Sensor TS1 was placed 2.5 m away from the thermobaric warhead with the intent of measuring the temperature within the explosion flame the radius of which, determined by the video still frames, was approx. 3 m. Unfortunately, the distance was too short for the sensor to survive the first SW, as shown in Fig. 7.

Sensor TS2 (20 m from the explosion epicentre/warhead) recorded a pulse generated between +40 and +50 ms (which was simultaneous with the contact of the SW front). Fig. 8 shows the temperature change trends recorded by the sensor during Explosions 2, 3 and 4. The slowly rising pre-pulse corresponded to the radial heating of the tungsten wire W by the explosion fireball. The steep pulse front corresponded to the transition of the SW, and its determined mean velocity is a close match to the values determined as explained above. After the SW front passage (up to approx. +100 ms), the temperature trends showed up to 3 peaks in ten+ millisecond intervals and a peak-valley height of 2-3 K (approx. 1/3 of the maximum). These peaks were within a period of approx. 6 ms and at an amplitude of approx. 0.3 K, clearly discernible from the oscillations imposed on the temperature trends. The oscillations originated from the instrumentation and were not related to any effect from the explosion, as proven by the fact that they were present from the start of the temperature trends.

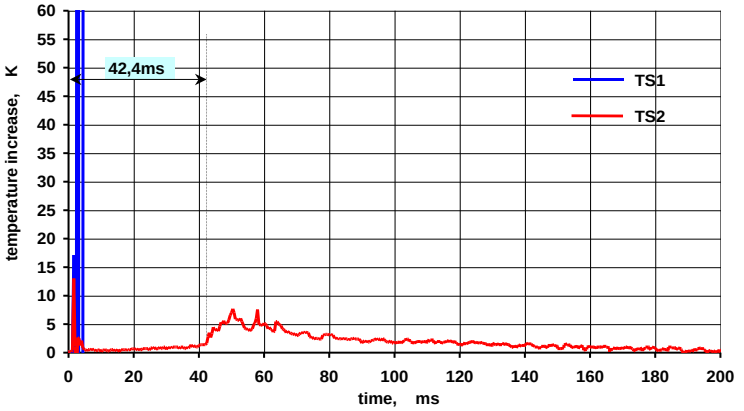

Fig. 7. Air temperature increase 2.5 m (Sensor TS1) and 20 m (Sensor TS2) from the detonating warhead; Sensor TS1 output break shown

The maximum possible value of the apparent temperature increases caused by mechanical deformation of the sensor (i.e. oscillating variations of the tungsten wire length) did not exceed 1.5 K, as estimated in Section 7.1. Hence, the peaks recorded by Sensors TS1 and TS2 were an actual thermal effect of the explosion, which at $t > 75$ ms for the overpressure at $r_{p1} = 5$ m was practically un-measurable (Fig. 3).

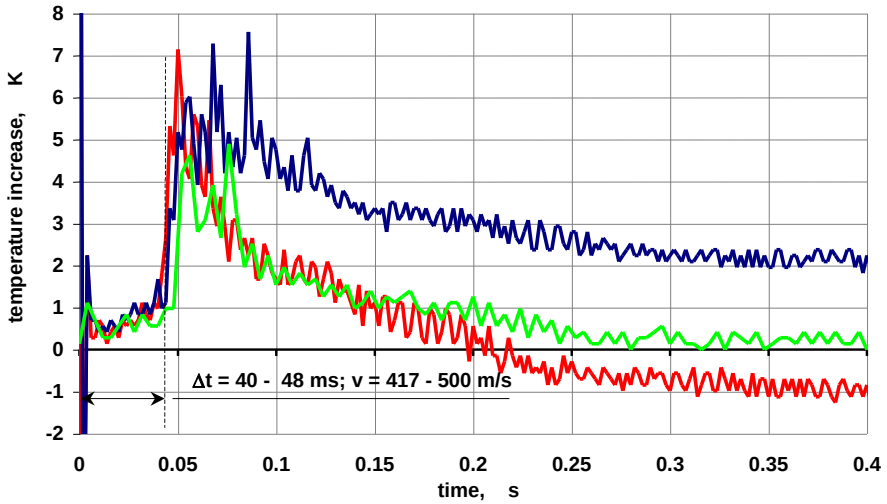

Fig. 8. Air temperature increase 20 m (Sensor TS2) from the detonating warhead; mean SW velocity shown at 20 m

This would preclude any forces that otherwise might have caused the stress oscillations and resulting changes in the tungsten wire length. On the other hand, generating the voltage changes corresponding to the temperature peaks shown in Fig. 5 by mechanical tensioning of the tungsten wire would require (5) extending its length 1.03 times (i.e. by > 2 mm from the original length of 70 mm), which would amount to plastic deformation of the tungsten wire, resulting in a changed voltage signal output. This effect was not observed.

The presence of the peaks mean that processes with comparable tungsten wire heating and cooling rates occurred at the tungsten wire mounting point. This suggests that the explosion cloud oscillated and there was a family of vortexes similar to toroids inside the cloud, rotating at the high circumferential velocity of gases (in the vertical plane) and periodically ejecting layers of hot gas towards the sensor, while inducing (from around the sensor) cold air in from outside the fireball. The rotary motion may have lasted much longer than the pressure pulses that caused it.

The response of the sensor to these processes are affected by the time constant of the device, one much lower than available in the thinnest commercially available thermocouples. Note, however, that the temperature output from the sensor depended on the sensor's time of residence in the diagnosed environment (which was the time of SW wash around the sensor), and the temperature increase recorded in the given time interval might be much smaller than the actual temperature increase of the gases (explosive reaction products).

7.1. Estimation of the temperature measurement error from mechanical tensioning of the sensor tungsten wire

The tungsten wire can be elongated by Δl from the original length l_0 with the wire volume unchanged only by reducing the wire diameter to d_1 so that $(d_1/d_d)^2 = l_0/(l_0 + \Delta l)$. The resulting resistance change is $\Delta R = l_0/\sigma/(\pi\ d_d^2/4)\ [(1 + \Delta l/l_0)^2 - 1]$

or
$$\Delta R / R_0 \approx 2\ \Delta l / l_0 \tag{6}$$

where σ – electrical conductivity of the tungsten wire.

7.1.1. Tungsten wire as a chord

Originally, the tungsten wire, W, was stress-free. The action of the transverse blast introduced longitudinal stress to the wire at a mean force N_T with transversal oscillations of the wire with a period τ_{osc}. The oscillation frequency, expressed as the first natural frequency of a chord, was $\omega = (2\pi / \tau_{osc}) = (\pi / l_0)\ (N_T / \rho / (\pi\ d_d^2 / 4))^{1/2}$ [8], $\rho = 19.2$ kgm^{-3}; hence $N_T \approx 0.04$ N.

This force corresponded to: (according to Hooke's law with Young's modulus $Y_W = 370$ GPa) the relative elongation $\Delta l / l_0 = 6.8 \times 10^{-5}$ and the change or resistance (6) $\Delta R / R_0 = 0.000136$ in the wire. Given (5), the apparent temperature change was $\Delta T \approx 0.03$ K.

7.1.2. Tungsten wire loaded with aerodynamic resistance

It was assumed that the tungsten wire was washed with the transverse flux of air at a density $\rho_g = 1.23$ kgm^{-3} and a mass velocity $u = v_{p1} / 2 \approx 400$ m/s (see Table 1). This velocity value was assumed with an excess. The transversal force acting on the wire with a surface area $S_\perp = l_0\ d_d$, was $P_D = c_D\ \rho_p\ u^2\ S_\perp / 2$. Given the relatively small diameter of the wire, air viscosity [9] was accounted for; hence the resistance force factor was $c_D = 1$, and $P_D = 0.115$ N after substitution of all relevant values. For the sake of simplification, the force was focused on the central part along the wire length, and given the geometry, Hooke's law and (5), the apparent temperature change (the measurement error) was $\Delta T \leq 1.3$ K.

8. CONCLUSIONS

1. Time trends of overpressure were recorded as occurring at the front of the blast waves generated by the explosion of the tested thermobaric warhead. It was found that the blast waves were shock waves in nature. The maximum overpressure values and specific times of blast wave propagation were measured.

2. The shock wave velocity values at the measurement points were determined, and the values served to verify by calculation the measured overpressure values. The verification confirmed a good agreement between the calculated and measured overpressure values.
3. The TNT equivalent was determined at approx. 3 kg TNT for the exploding charge and corresponding to the energy transferred to the shock wave.
4. The personnel strike radius by the shock wave from the thermobaric warhead was determined to be approx. 13 m.
5. Based on the slow-motion video recording, a very good axial symmetry was found in the dispersal of explosion products and non-converted material of the thermobaric warhead in Stage 1 of the explosion.
6. The maximum diameter of the explosion fireball (i.e. the extreme temperature area) was determined at approx. 5.5 m.
7. The measured temperature increase outside the blast wave front was at least 50 K at 5 m and at least 7 K at 20 m from the explosion epicentre.
8. The duration of the overpressure positive phase outside the shock wave front was found to be 1.5 times longer (6 ms) than in an equivalent classic explosive; the duration of the extremely high temperature area was ten+ times longer (approx. 100 ms).
9. Based on the recording of the temperature and pressure values, the assumed multi-phase nature of a thermobaric warhead explosion was proven. Pressure and temperature oscillations were proven to exist within an area near to the explosion fire ball. They were affected by the intense exchange of gases in the area.

REFERENCES

[1] Barcz Katarzyna, Waldemar A. Trzciński. 2010. „Materiały wybuchowe termobaryczne i o podwyższonej zdolności podmuchowej". *Biuletyn Wojskowej Akademii Technicznej* LIX (3) : 7-39.

[2] Borkowski Jacek, Eugeniusz Milewski, Bogdan Zygmunt. 2007. „Amunicja termobaryczna – rodzaj amunicji przestrzennej". *Problemy Techniki Uzbrojenia* 102 : 89-100.

[3] Faryński Andrzej, Konrad Mackiewicz, Zbigniew Ziółkowski. 1994. „Rejestracja impulsów ciśnienia za frontem fali uderzeniowej i oszacowanie równoważników trotylowych detonowanych objętościowych ładunków aerozolowych". *Biuletyn Instytutu Technicznego Wojsk Lotniczych* 11772/I : 1-37.

[4] Faryński Andrzej, Andrzej Długołęcki, Zbigniew Ziółkowski. 2008. „Pomiary parametrów fali uderzeniowej wytwarzanej przez wybuch głowicy niekierowanego lotniczego pocisku rakietowego 70 mm". *Biuletyn Wojskowej Akademii Technicznej* LVII (3) : 173-180.

[5] Gilliam Jason. 2005. TBX Evaluation Testing in the M151 Warhead as Risk Reduction for the APKWS. Presented at *2005 NDIA Missiles & Rockets Symposium*.
[6] Długołęcki Andrzej, Andrzej Faryński, Zbigniew Ziółkowski. 2011. „Pomiary temperatury powietrza w rejonie wybuchu głowicy RA-79 niekierowanego lotniczego pocisku rakietowego S-7". *Biuletyn Wojskowej Akademii Technicznej* LX (2) : 29-37.
[7] Epov B.A. 1974. *Osnovy vzryvnogo dela*. Moskva: Voen. Izdat. Min. Obor. SSSR.
[8] Dżygadło Zbigniew, Sylwester Kaliski, Ludwik Solarz, Edward Włodarczyk. 1966. *Drgania i fale w ciałach stałych*, Warszawa: Wydawnictwo PWN.
[9] Woźniak S. 1996. "Badania analityczne ruchu ziaren pyłu w odpylaczu osiowym ze stycznym doprowadzeniem powietrza". *Biuletyn Wojskowej Akademii Technicznej* XLV (2) : 59-68.

Badanie czynników rażenia wybuchu głowicy termobarycznej

Andrzej DŁUGOŁĘCKI, Andrzej FARYŃSKI, Tomasz KLEMBA, Łukasz SŁONKIEWICZ, Zbigniew ZIÓŁKOWSKI

Instytut Techniczny Wojsk Lotniczych, Warszawa
ul. Księcia Bolesława 6, 01-494 Warszawa

Streszczenie. W artykule przedstawiono metodę i wyniki pomiarów impulsów ciśnienia i efektów termicznych generowanych przez wybuch głowicy termobarycznej rakiety niekierowanej. Wyznaczono ciśnienia i prędkości fal uderzeniowych, równoważniki trotylowe detonowanych głowic oraz promienie rażenia siły żywej przez falę uderzeniową, oszacowano przyrosty temperatury na froncie fali uderzeniowej.
Słowa kluczowe: mechanika, wybuch termobaryczny, fala uderzeniowa, prędkość fali uderzeniowej, impuls ciśnienia